Defense Technical Information Center Compilation Part Notice

ADP012400

TITLE: Energy Transfer Dynamics in the A[0 sub u[+]] State of Bi2

DISTRIBUTION: Approved for public release, distribution unlimited

This paper is part of the following report:

TITLE: Gas and Chemical Lasers and Intense Beam Applications III Held in San Jose, CA, USA on 22-24 January 2002

To order the complete compilation report, use: ADA403173

The following component part numbers comprise the compilation report:
ADP012376 thru ADP012405

Energy transfer dynamics in the $A(0_u^+)$ state of Bi_2

Joseph L. Cox,[1] Michael W. Dolezal,[2] Robert E. Franklin,[3] and Glen P. Perram[4]
Air Force Institute of Technology

ABSTRACT

Laser induced fluorescence, pulsed and CW, techniques have been used to study energy transfer within the $A(0_u^+)$ state of Bi_2. In particular, electronic quenching in the vibrational levels near predissociation, v'=18-25, have been examined for rare gas and nitrogen collision partners. The quenching from non-predissociated levels is independent of vibrational state and are rather rapid, 2.3 – 8.5 x 10^{-11} cm^3/molecule-s for v'=22. The quenching from the first significantly predissociated level, v'=23, is even faster with rate coefficients ranging from 7.4 – 15.7 x 10^{-11} cm^3/molecule-s. Heterogeneous predissociation is very rapid for $21 \leq v' \leq 39$, with rates, $\Gamma = k_{pd}(v')\ J\ (J+1)$, of k_{pd} as large as 1.5 x 10^5 s^{-1}. Vibrational-to-translational energy transfer probabilities for the lowest vibrational levels, v'=0-4, range from 0.75 – 1.75% per collision, considerably lower than would be anticipated for these highly non-adiabatic collisions. Spectrally resolved emissions from collisionally populated rotational levels of $Bi_2(A,v'=1)$ were observed for helium, neon and argon collision partners after laser excitation of the high rotational levels J'=171, 201, and 231. Total rotational removal rates from the initially prepared state range from 2.8 – 8.9 x 10^{-10} cm^3/molecule-s. Collisional population of rotational states with $|\Delta J| \leq 56$ was observed at pressures of 0.09 – 1.4 torr. The state-to-state rates are adequately modeled by the energy based statistical power gap law.

Keywords: bismuth dimmer, spectroscopy, predissociation, quenching, vibrational energy transfer, rotational energy transfer, laser induced fluorescence

1. INTRODUCTION

Several optically pumped Bi_2 (A-X) lasers were demonstrated in the late 1970's and early 1980's with photon efficiencies approaching 20%.[1-2] Bismuth dimers also play an important role in the $NF(a^1\Delta)$ - BiF laser system.[3] The current work reports on the collisional dynamics of the Bi_2 $A(0_u^+)$ state from a series of laser induced fluorescence experiments.[4-6]

The bismuth dimer is the heaviest stable diatom and offers a unique opportunity to study the collisional dynamics of states with high angular momentum, as well as vibrational energy transfer in strongly coupled systems. The vibrational frequency is low, $\omega_e \simeq 132$ cm^{-1}, and the Bi_2 – He collision involves a high relative speed at room temperature, yielding a ratio of collision time to the vibrational period of ~ 0.06. The very low rotational constant for Bi_2 offers significant populations in rotational states above J=200 even at modest temperatures (T≈300 K).

The spectroscopy of the Bi_2 $A(0_u^+) - X(0_g^+)$ system is well characterized, particularly for the low lying vibrational levels.[7-9] The radiative lifetime of $Bi_2(A)$ is 272 - 595 ns for v'<20, and a strong predissociation is observed near v'=27.[10-11] However, the collisional dynamics of $Bi_2(A)$ is less studied. The radiative rates,[5,10-11] quenching from a few (v', J') levels,[11] and vibrational energy transfer in the lowest vibrational levels[12] have previously been reported. In addition, several Bi_2(A-X) lasers have been demonstrated.[1-2]

[1]joseph.cox@eglin.af.mil; phone 1 850 8821724 x 117; Fax 1 850 882 1717; http://www.afrl.af.mil; Air Force Research Laboratory/MNGS, 101 West Eglin Blvd Suite 287, Eglin AFB, FL 32542-6810 [2]michael.dolezal@aftac.patrick.af.mil; phone 321 494-9610; http://www.aftac.gov; Air Force Technical Applications Center/TAT-A, 1030 S Highway A1A, Patrick AFB, FL 32925;[3]robert.franklin@wpafb.af.mil; phone 937 674 8035x3903; https://www.asc.wpafb.af.mil/asc/; Aeronautical Systems Center/GRI, 2145 Monahan Way, Wright-Patterson AFB, OH 45433; [4]glen.perram@afit.edu; phone 1 937 255 3636 x 4504; Fax 1 937 255 2921; http://www.afit.edu; Air Force Institute of Technology/ENP, 2950 P Street, Wright-Patterson AFB, OH 45433-7765

Gas and Chemical Lasers and Intense Beam Applications III, Steven J. Davis, Michael C. Heaven, Editors, Proceedings of SPIE Vol. 4631 (2002) © 2002 SPIE · 0277-786X/02/$15.00

2. EXPERMENT

The steady-state laser induced fluorescence apparatus is depicted in Figure 1. A Coherent model 899-29 ring dye laser with Rhodamine 590 dye was used to selectively excite the $A(0_u^+)$ state. Laser excitation spectra were recorded,[4,8] indicating the excitation of a pure (v',J') state. The dye laser was operated with a power of 0.3 – 0.9 mW and the laser linewidth was less than 100 MHz. A McPherson 1.3m monochromator with a Princeton Instruments model 1024 SR/B optical multichannel analyzer (OMA) was used to resolve the laser induce fluorescence with a resolution of 0.5 cm^{-1} and a bandwidth of 225 cm^{-1}. The spectral response of the OMA was calibrated with a blackbody source at 1266 K.[4]

The bismuth dimer was generated by heating a small sample of granular bismuth (Mallinckrodt, 99.8%) in a 1 cm aluminum oxide crucible and tungsten basket heater to 900 – 1000 K. Such an apparatus typically produces about 33% atomic bismuth and 66% bismuth dimer.[11] The fluorescence cell consisted of a 6–way (3.8 cm diameter x 20 cm length) stainless steel cross with quartz windows along the laser axis and for viewing the laser induced fluorescence. The fluorescence cell could be evacuated to 8 x 10^{-6} Torr via an oil diffusion pump, and exhibited a room temperature leak rate of less than 3 mTorr/hour. Typically, the cell was operated with 0.1 –12.0 Torr of rare gases (99.996%) added to induce energy transfer. The rate of out-gassing with the basket heater on was 1-2 mTorr/min. The cell pressure was monitored with MKS model 390 10 Torr and model 122A 100 Torr capacitance manometers.

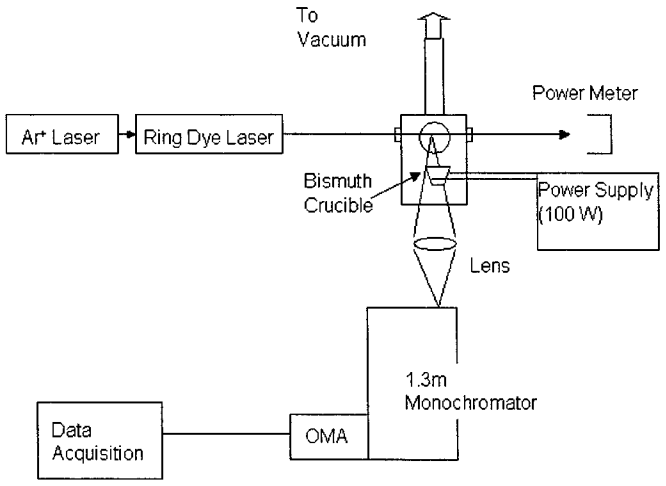

Figure 1. CW laser induced fluorescence apparatus.

For the pulsed laser induced fluorescence experiments, a Nd:YAG pumped dye laser using Coumarin 460, 480 and 500 dyes with typical pulses energies of 10-25 mJ was used to excite $Bi_2(A)$ in a similar vacuum apparatus. The side fluorescence was detected with an RCA C30134 photomultiplier tube and recorded on a LeCroy 940 350 MHz digital oscilloscope.

3. RESULTS

The experiments are grouped into four sections: (1) pulsed Laser Induced Fluorescence (LIF) lifetimes to study predissociation, (2) electronic quenching rates from time-resolved emission profiles, (3) CW LIF studies of vibrational energy transfer, and (4) CW LIF rotational energy transfer for high J within v'=1.

3.1 Predissociation

The laser excitation spectrum from 18,725 to 21,950 cm^{-1} was recorded with a Nd:YAG pumped dye laser at 0.3 cm^{-1} spectral resolution. A segment of the spectrum is provided in Figure 2. The sudden onset of predissociation is seen for v' ≥ 22 as a dramatic decrease in the extent of the rotational distribution. The red shaded bands are reduced to narrow features near the band head. In fact, for most of the predissociated levels, no resolved rotational structure can be identified.

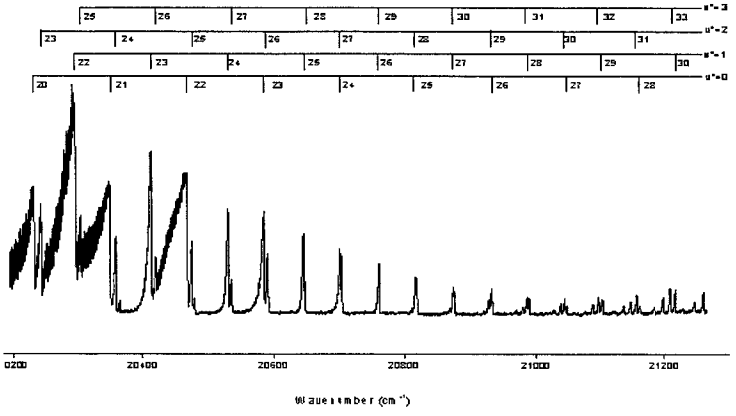

Figure 2. Pulsed laser excitation spectrum with (v', v") band heads indicated.

The fluorescence intensity as a function of time for v'=21-22 decays exponentially, as shown in Figure 3. The logarithmic plot illustrates single exponential behavior for at least 6 e-folds. By examining the dependence of the decay rates on pressure, the collisionless decay rates were determined. A plot of these collisionless decay rates as a function of rotational state is shown in Figure 4. The transition rates for heterogeneous predissociation are given by $\Gamma_o = 1/\tau_r + k_{pd}(v')J(J+1)$, where τ_r is the radiative lifetime and $k_{pd}(v)$ is a measure of the strength of the predissociation and is dependent on vibrational level.

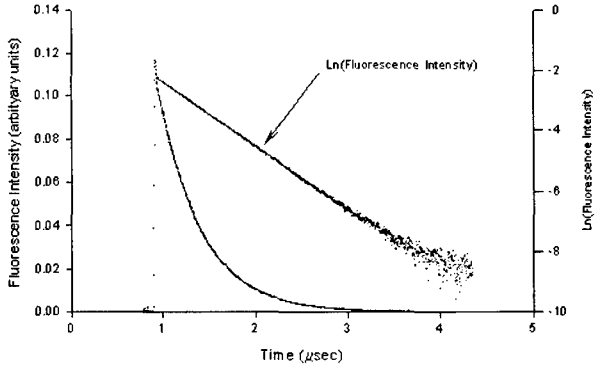

Figure 3. Decay lifetime for v'=21, J'=50 at 100 mTorr.

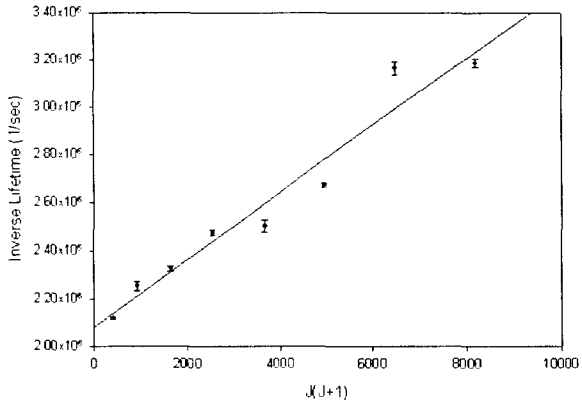

Figure 4. Rotational dependence to predissociation in v'=21.

For v'>22, the predissociation is sufficiently strong that only rotational states near the band head have significant emission intensity, and these rotational levels cannot be isolated by the pump laser. To extract predissociation rates, k_{pd}, for theses states, we have employed a spectral simulation.[5] Briefly, the intensity of each rotational line is modeled, including the effects of predissociation , and convolved using the laser linewidth to simulated the laser excitation spectra. By comparing the synthetic and observed spectra, a best estimate for the predissociation rate is determined. A summary of the resulting predissociation rates is provided in Figure 5.

The predissociation in $Bi_2(A)$ is very strong, exhibits a broad dependence of vibrational level and yields no stable vibrational levels above v'=22.

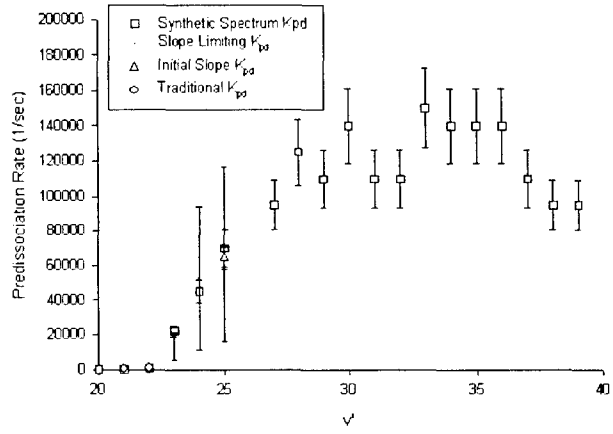

Figure 5. Predissociation rate constant, k_{pd}, as a function of vibrational level.

3.2 Electronic Quenching

The pressure dependence of the total fluorescence decay rates establish the electronic quenching rates, $\Gamma = \Gamma_o + k_q[M]$, where [M] is the concentration of the added buffer gas. For the vibrational levels below the onset of predissociation, v'=18-22, the electronic quenching rates for helium are independent of vibrational level, as shown in the Stern-Volmer plot of Figure 6. The probability for quenching, defined as the ratio of the observed quenching rate to the gas kinetic rate, depends linearly on reduced mass of the collision pair, as shown in Figure 7.

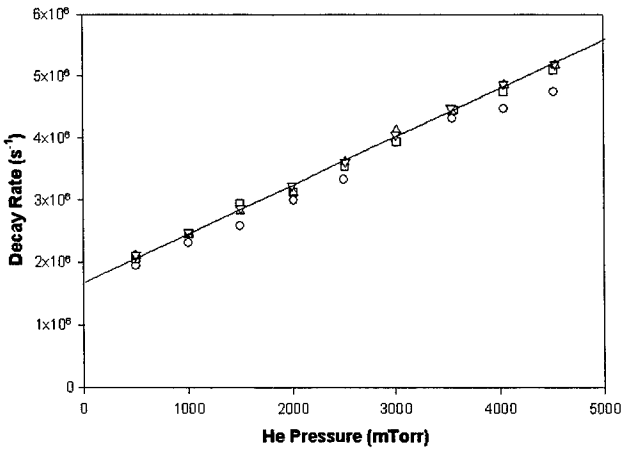

Figure 6. Electronic quenching for v'=18 (o), 19 (□), 20 (Δ) and 21 (∇).

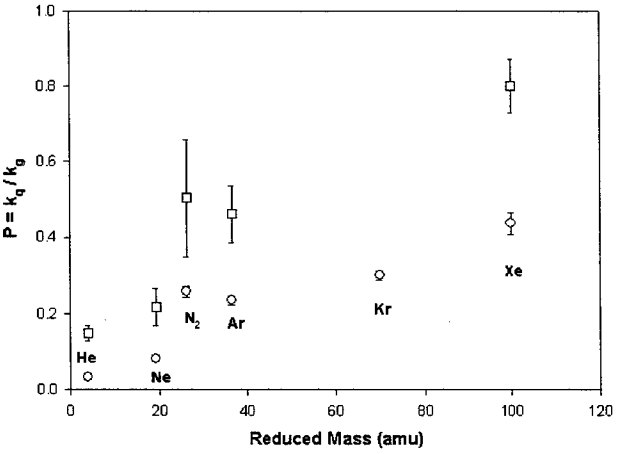

Figure 7. Quenching probability for v'=22 (o) and v'=23 (□).

The quenching from v'=23 are about twice the rates for v" ≤ 22. Vibrational ladder climbing to higher, strongly predissociated vibrational states and rotational energy transfer to higher J within v'=23 likely contributes to the increased total quenching.

Table I.
Electronic Quenching for v'=22

Buffer Gas, M	Reduced Mass (amu)	Quenching Rate, k_q (10^{-11} cm^3 / molecule-s)	Gas Kinetic Rate (10^{-10} cm^3/molecule-s)	Probability, P
He	3.96	2.27 ± .16	7.03	0.0323 ± 0.0023
Ne	19.3	2.80 ± .19	3.41	0.0822 ± 0.0056
Ar	36.5	6.65 ± .35	2.84	0.2340 ± 0.0123
Kr	69.8	6.39 ± .25	2.13	0.2998 ± 0.0115
Xe	99.9	8.51 ± .55	1.95	0.4362 ± 0.0282
N_2	26.2	8.03 ± .45	3.12	0.2574 ± 0.0145

Quenching rates for v' > 23 were not reliably obtained, due to the very fast predissociation. Figure 8 illustrates the decay waveforms for v' = 22 - 25. The very fast decay rates for v' = 24 -25 exceed 5 x 10^7 s^{-1}, or $\tau \leq 20$ ns. The pulsed dye laser has a pulse width of about 10 ns, and does not allow for sufficient temporal resolution to extract reliable quenching rates.

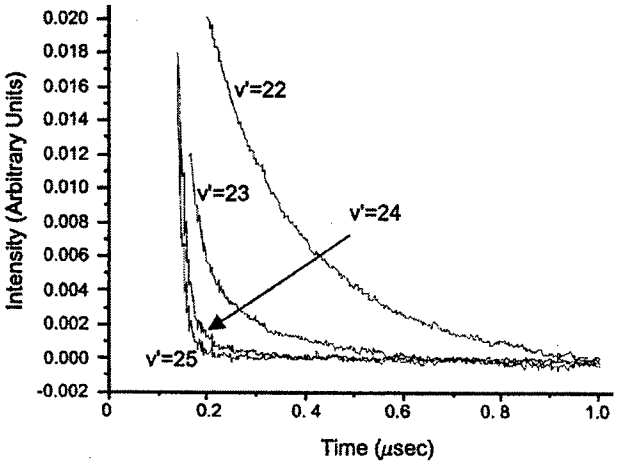

Figure 8. Lifetimes for He at 3 Torr.

3.3 Vibrational Energy Transfer

A spectrum showing the effects of vibrational energy transfer after laser excitation of v'=3 is shown in Figure 9. Band heads are labeled (v',v") for some of the more prominent features. The spectrum was recorded for a neon buffer gas at 4.76 Torr and significant populations are observed in v'=0-2, indicating rapid vibrational energy transfer. The P-R doublet emission from the laser excited v'=3, J'=104 level is evident in the (3,8) band. This P-R doublet structure is not clearly evident in the other two bands originating from v'=3 due to low Franck-Condon factors. A spectral region with low Franck-Condon factors from the laser excited, or parent, state is desirable for quantifying the population in collisionally populated, or satellite states. Similar spectra were recorded for He, Ne, Ar, Kr, and Xe buffer gases at pressures of 0.1 – 12.0 torr. In order to determine the populations in various vibrational levels, synthetic spectra were fit to the observed spectra. The comparison between the observed and fit spectra, as shown in Figure 9, is generally adequate. The differences are largely attributed to vibrational bands excluded from the spectral simulation.

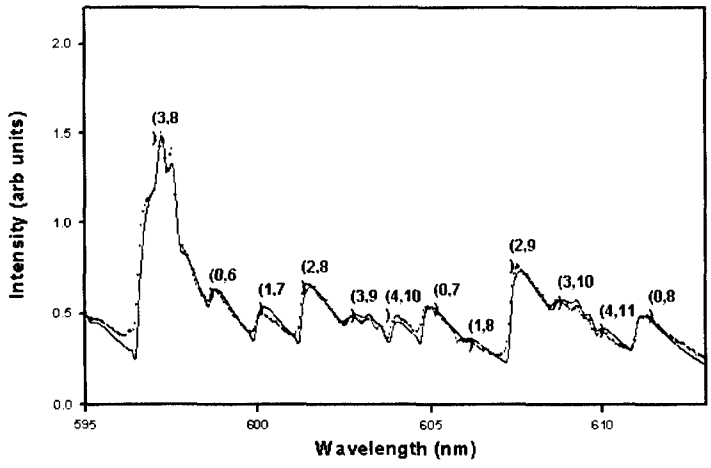

Figure 9. CW LIF vibrationally resolved spectrum and simulation. Band heads are indicated (v',v").

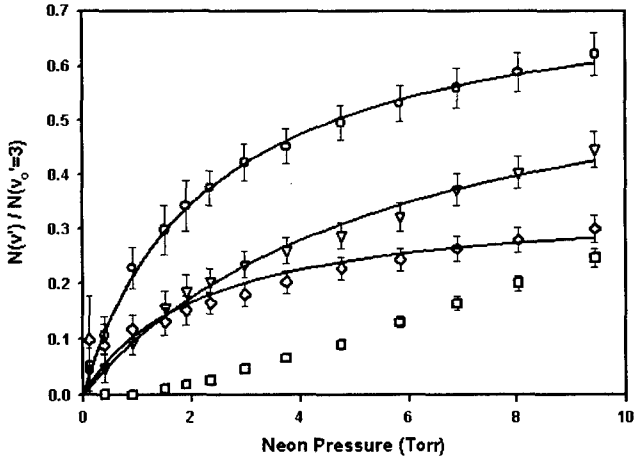

The relative vibrational populations after laser excitation of v'=3 as a function of neon buffer gas pressure are shown in Figure 10. The populations in v' = 4, 2, and 1 increase linearly at low pressures, but exhibit curvature for pressures above a few Torr due to multiple collisions that remove population from the satellite state. The relative populations in the satellite levels v'=2 and 1 near 10 Torr is approximately 1.3, as compared to the equilibrium value of $N(v'=2)/N(v'=1) = \exp[-\omega_e/kT] \approx 0.5$. Significant vibrational relaxation has occurred at 10 Torr buffer gas pressure, but the distribution is still far from equilibrium. The population in v'=0 exhibits curvature at low pressures, indicative of population cascading through intermediate vibrational levels.

Figure 10. Vibrational population distributions as a function of neon buffer gas pressure after laser excitation of v'=3. The observed populations for: (O) v'=2, (∇) v'=1, (◊) v'=4, and ( ) v'=0 are fit to: (——) equation (4), and (---) the constrained rate matrix of equation (2).

In order to extract state-to-state vibrational transfer rate coefficients from data similar to that shown in Figure 10 , a steady-state analysis of the master rate equation is required. The master rate equation for the population in vibrational level v is:[4,6]

$$\frac{dN_v}{dt} = S\delta_{v,v_0} + \sum_w R_{vw} N_w \qquad (1)$$

where w is the quantum number for other vibrational levels of $Bi_2(A)$, S is rate for laser excitation of the parent level v_o, and R_{vw} denotes the rate coefficient matrix:

$$R_{vw} = k_{VT}(w \rightarrow v)[M] - \delta_{vw}\left\{\Gamma_r + k_Q(v)[M] + \sum_w k_{VT}(v \rightarrow w)[M]\right\} \quad (2)$$

The goal of this work was to extract the rate coefficients for vibrational transfer from state w to state v, $k_{VT}(w \rightarrow v)$, from the rate matrix, R_{vw}. The radiative decay rate for $Bi_2(A, v' \leq 3)$ is $\Gamma_r = 1.6 - 2.3 \times 10^6\ s^{-1}$.[11] For a given rate matrix, R_{vw}, the relative steady-state populations can easily be determined as:

$$\frac{N_v}{N_{v_o}} = \frac{k_{VT}(v_o \rightarrow v)[M]/\Gamma_r}{1 + [k_Q(v)[M] + \sum_w k_{VT}(v \rightarrow w)][M]/\Gamma_r - \sum k_{VT}(w \rightarrow v)\left[\frac{N_w}{N_v}\right][M]/\Gamma_r} \quad (3)$$

The third term in the denominator of equation (3) represents multiple collisions that populate the observed vibrational level. In general, this term possesses a complicated pressure dependence. However, at moderate pressures where multiple collisions are not dominant, equation (3) reduces to the form:

$$\frac{N_v}{N_{v_o}} = \frac{Ax}{1 + Bx} \quad (4)$$

where $A = k_{VT}(v)/\Gamma_r$, $B = (k_Q(v) + \sum_w k_{VT}(v \rightarrow w))/\Gamma_r$, and $x = [M]$.

Figure 10 illustrates a least-square fit of equation (4) to the data, providing an initial estimate of the state-to-state V-T rate coefficients, as reported for neon in Table II. The data for v' = 0 can not be adequately represented by equation (4), since single collision transfer involving $\Delta v = -3$ is insignificant. Similar data were recorded for laser excited states v' = 1-4 and for He, Ne, Ar, Kr, and Xe buffer gases.

Table II.
Vibrational transfer rate coefficients for neon.
(10^{-12} cm^3/molecule-s)

v	k_{VT}^{Ne}(v→v-1) (from fit to equation (4))	k_{VT}^{Ne}(v→v-1) (from rate matrix model)	k_{eq}	f
1	6.3 ± 0.7	6.2 ± 0.7	< 0.9	0.16
2	9.6 ± 0.7	9.6 ± 0.7	< 2.9	0.10
3	15.1 ± 1.4	14.1 ± 1.4	< 3.3	0.12
4	19.6 ± 3.5	19.2 ± 3.5	< 3.3	0.05

In order to refine the determination of the vibrational transfer rate coefficients, the full rate matrix of equation (2) is utilized. To reduce the number of independent matrix elements, detailed balancing is used to specify transitions that increase vibrational energy, linear scaling of the vibrational transfer rate coefficients with vibrational quantum number as predicted for harmonic oscillators is applied, transfer involving multi-quanta is assumed to be a fixed fraction, f, of the $\Delta v = -1$ rate, and the rates for $|\Delta v| \geq 3$ are neglected. The electronic quenching and radiative rates are assumed independent of vibrational level. By varying the quantities k_{VT}(v→v-1), k_q and f, a single rate matrix which best represents the full set of spectrally-resolved laser induced fluorescence data can be established. The corresponding predictions for v'=4,2, and 1 are quite similar to the fits from equation (4). The resulting rate parameters for neon collisions are provided in Table I. Collisions with the remaining rare gases were studied in somewhat less detail. The vibrational levels examined and resulting rate coefficients are reported in Table III.

Table III.
Fundamental vibrational transfer rate coefficients for rare gases.
(10^{-12} cm^3/molecule-s)

Gas	v_o'	$k_{VT}(v \rightarrow v\text{-}1)$	$k_{VT}(1 \rightarrow 0)$	$\sigma_v(1,0) / \sigma_g$
He	2	10.6 ± 1.5	5.3 ± 0.7	0.0075
Ne	1-4	(see Table I)	4.8 ± 0.9	0.0142
Ar	3	7.6 ± 1.2	2.5 ± 0.4	0.0089
Kr	2	4.8 ± 0.7	2.4 ± 0.4	0.0112
Xe	2	6.8 ± 1.3	3.4 ± 0.7	0.0175

The Schwartz, Slawsky, and Herzfeld (SSH) theory[13] successfully predicts the probability for vibrational transfer (V-T), particularly the scaling with mass and vibrational frequency, under a wide range of conditions.[14] The SSH theory depends on the first-order Born approximation, models a harmonic oscillator perturbed by an exponential interaction potential, and assumes a relatively non-impulsive, or near adiabatic, collision. The SSH theory predicts the probability for vibrational transfer as:[14]

$$P(1,0)=\frac{\sigma(1,0)}{\sigma_g}=M\left(\frac{\Theta'}{\Theta}\right)\left(\frac{\Theta'}{T}\right)^{1/6}\exp\left[-3/2\left(\frac{\Theta'}{T}\right)^{1/3}+\left(\frac{\Theta}{2T}\right)+\left(\frac{\varepsilon}{kT}\right)\right] \quad (5)$$

where

$$M=\sqrt{\frac{2\pi}{3}}\frac{2m_A{}^2 m_B m_C}{(m_B+m_C)(m_A+m_B)^2\mu}$$

μ=collision pair reduced mass=$m_A(m_B+m_C)/(m_A+m_B+m_C)$

$\Theta'=4\pi^2L^2(2\pi c\omega_e)^2\mu/kT$

$\Theta=hc\omega_e/kT$

ω_e=fundamental vibrational frequency (cm^{-1})

ε=potential well depth

L=potential interaction length

σ_g=gas kinetic or hard sphere cross-section

Surveying the existing database of V-T transfer for the diatomic halogens indicates a deficiency of the SSH theory for highly impulsive collisions.[15] By converting the observed V-T transfer rate coefficients to a transition probability, using the specified masses, vibrational frequency, and translational temperature, and assuming a small well depth, $\varepsilon/kT \approx 0$, the interaction lengths, L, required to satisfy equation (5) are specified displayed in Figure 11. For adiabaticity, $\xi=c\omega_e L(\pi\mu/8kT/)^{1/2} > 0.5$, the interaction lengths are in the range L = 0.25-0.10, which is typical for V-T transfer.[14] However, the most impulsive collisions, particularly the $Bi_2(A)$ – He interaction, require unreasonably large interaction lengths. In other words, the SSH theory over-predicts the probability for V-T transfer involving highly impulsive conditions. A large interaction length artificially reduces the prediction to generate agreement with the observed rates.

There are several approximations made in the SSH theory that depend on near adiabatic conditions: (1) the first-order Born approximation is used to compute the transition probability, (2) the matrix elements for the exponential interaction potential are approximated by a first-order Taylor series, and (3) when averaging over the velocity distribution, the approximation $\text{csch}^2(2\pi^2 c\omega_e L/v) \approx 4\exp(-4\pi^2 c\omega_e L/v)$ is employed. The latter two approximations can be improved,[16-17] but the differences are not sufficiently large to account for the interaction lengths computed in Figure 7. The large interaction lengths for the most impulsive collisions ($\xi < 0.3$) appear to result from the failure of the first-order Born approximation.

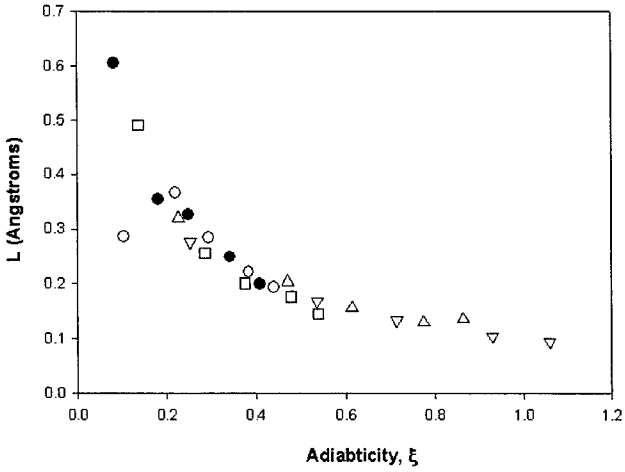

Figure 11. The interaction length derived using the SSH theory of equation (15) from V-T rate coefficients observed for: (•) Bi_2(A) (present work), (O) Br_2(B) (ref 21), ( ) BrCl(B) (ref 18), (Δ) BrF(B) (ref 21), and (▽) IF(B) (ref 19). To evaluate the adiabaticity, a constant value for the interaction length was chosen, L = 0.02 nm.

3.4 Rotational Energy Transfer

Similar experiments have been performed with rotational state resolution. The spectrally resolved emission from the v'=1 → v"=5 band after excitation of v'=1, J'=171 in the presence of 0.855 torr of helium is shown in Figure 12. The strong P-R doublet emission from the laser populated state is clearly evident. The weaker satellite transitions are from the collisionally populated rotational states. Emission is observed only from even rotational levels because the nuclear spin is not readily altered by collisions.[22] For J'< 140, a near coincidence of the P(J) and R(J+14) lines precludes complete spectral isolation. The rotational transfer rates are quite rapid, with significant population in the satellite states even at low buffer gas pressures.

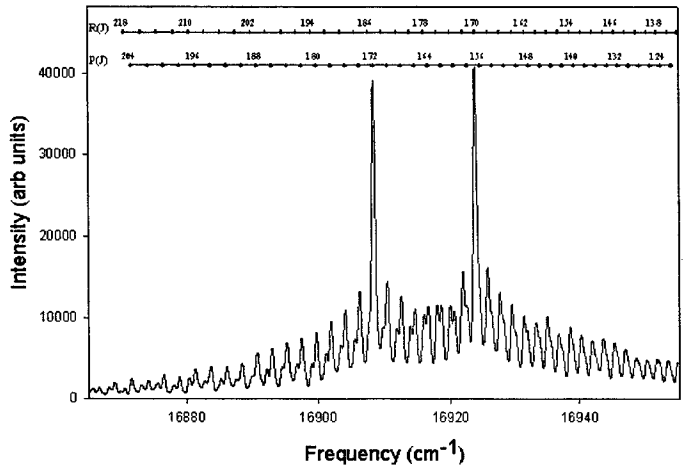

Figure 12. Spectrally resolved Bi_2(A-X) laser induced fluorescence from the v'=1 to v"=5 band in the presence of 855 mTorr of helium buffer gas after laser excitation of v'=1, J=171.

A plot of the population in the satellite level J'=165 relative to the population in the parent level, J'=171, is shown as a function of helium buffer gas pressure in Figure 13. The error bounds indicated in Figure 13 are obtained from the uncertainties in the amplitudes from the spectral fits. Similar data were obtained for initially pumped states J_o'=171, 201 and 231 and satellite states $-56 < \Delta J < +44$. This data was analyzed with a steady-state analysis similar to that described above for vibrational energy transfer and typical rate constants are provided in Figure 14.

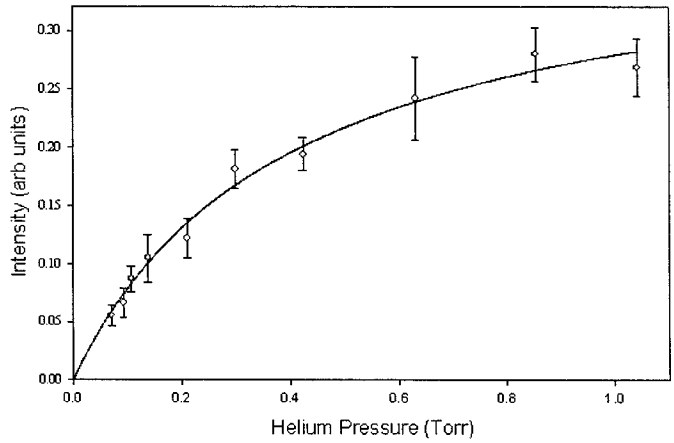

Figure 13. Plot of the population of the satellite J'=165 rotational level relative to the parent state (J'=171) for collisions with helium buffer. The solid line is a least-squares fit to the data using an analysis similar to equation (4).[4]

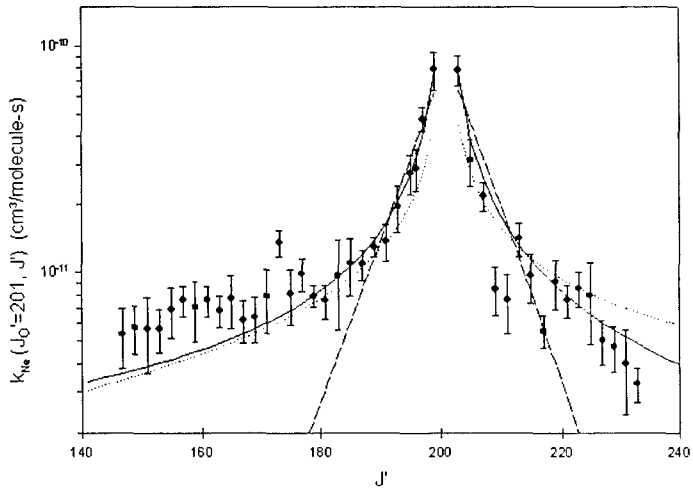

Figure 14. State-to-state rotational energy transfer rate constants for Ne after laser excitation of v'=1, J'=201. Three scaling law fits are also shown: (—) SPG1, (....) SPG2 and (---) EGL1.

Several empirical relationships have been proposed to describe the scaling of the state-to-state rotational energy transfer rate constants with rotational quantum number.[23-24] A variety of these fitting laws have been applied to the current data in an attempt to evaluate those which adequately represent the data. In Figure 14, a fit of the SPG1, SPG2 and EGL1 fitting laws are shown.[4] The exponential gap law fails for all the initially prepared J_o levels and buffer gas studies observed in the present work. The EGL1 and EGL2 fitting laws can be made to represent either the rotational levels near the pumped state, or for larger ΔJ, but not both. The statistical power gap laws do provide an adequate representation of the data for all J_o and all three collision partners. The M_J conserving form of the statistical factor *f(J)* (SPG1) provides a fit standard error of 20-50% less than the completely randomized factor (SPG2) and in all cases provides a better fit. Fit parameters for the statistical power gap law (SPG1) are summarized for each of the collision partners in Table II.

Table II.

Fit parameters for the statistical power gap scaling law, SPG1.

Collision Partner	(v',J_o')	B (10^{-8} cm³/molecule-s)	γ
He	(1,171)	5.45 ± 1.17	0.944 ± 0.030
He	(1,201)	3.85 ± 0.59	0.902 ± 0.021
He	(1,231)	2.79 ± 0.50	0.834 ± 0.025
Ne	(1,201)	5.00 ± 1.23	0.968 ± 0.034
Ar	(1,201)	1.25 ± 0.50	0.786 ± 0.042

4. CONCLUSIONS

A systematic study of predissociation in Bi_2(A) has been completed, indicating a curve crossing at v'=23. The predissociation is very strong, exhibits a broad dependence of vibrational level and yields no stable vibrational levels above v'=22. Electronic quenching is rapid, with rates 0.03 – 0.8 time the limiting gas kinetic value. Quenching is independent of vibrational level to the predissociation limit, but increase significantly at v'=23. Vibrational energy transfer in the lowest vibrational levels of Bi_2(A) is rapid, although somewhat less than predicted by the SSH theory. The Bi_2(A) potential is nearly harmonic, leading to a linear scaling of the vibrational transfer rates with vibrational quantum number and a low probability for multi-quantum transfer. Interaction lengths for bismuth dimer – rare gas collisions are consistent with those derived for the diatomic halogens when the collision pair exhibits the same adiabaticity. Rotational energy transfer within Bi_2(A) is rapid, constrained to ΔJ = even by parity conservation, and best represented by the statistical power gap scaling law with M_J conservation. Single collision population of rotational levels with $|\Delta J| \leq 52$, $\Delta E > 300$ cm^{-1}, is readily apparent. Even for these very high rotational states, with large angular momentum, the energy based scaling laws appear to provide a better representation of the rates than the energy corrected sudden with a power law for the angular momentum scaling.

REFERENCES

1. W.P. West and H.P. Broida *Chem. Phys. Lett.* **56** 283 (1978).
2. S. Drosch and G. Gerber *J. Chem. Phys.* **77** 123 (1982).
3. D.J. Benard *J. Appl. Phys.* **74** 2900 (1993).
4. R.E. Franklin *"Spectroscopic and Kinetic Studies of Bismuth Dimers"*, PhD Dissertation, Air Force Institute of Technology, AFIT/DS/ENP/97-04 (1997).
5. Michael W. Dolezal *Spectroscopic Constant, Lifetimes and Predissociation Rates for Bi_2 $A(0_u^+)$*, Ph.D. Dissertation, Air Force Institute of Technology, AFIT/DS/ENP/01-01 (2001).
6. Joseph L. Cox, *Electronic Quenching of the $A(0_u^+)$ State of Bi_2*, M.S. Thesis, Air Force Institute of Technology, AFIT/GAP/ENP/01M-02 (2001).
7. 10. R.F. Barrow, F. Taher, J.D. Incani, C. Effantin, A.J. Ross, A. Topovzkhanian, G. Wannous, and J. Verges, *Molecular Physics* **87** 725 (1996).
8. R.E. Franklin and G.P. Perram, *J. Molec. Spectrosc.* **194** 1 (1999).
9. G. Gerber, Honinger, and J. James *Chem. Phys. Lett.* **85** 415 (1982).
10. J.M. Blondeau, G. Gandara, P. Carette and J. Messelyn *Chem. Phys. Lett.* **71** 246 (1980).
11. G. Ehret and G. Gerber *Chem. Phys.* **66** 27 (1982).
12. Robert E. Franklin and Glen P. Perram, *"Collisional Dynamics of Bi_2 $A(0_u^+)$. I. Quantum-Resolved Vibrational Energy Transfer for v'=0-4"*, Journal of Chemical Physics, **111**, 5757 (1999).
13. R.N. Schwartz, Z.I. Slawsky, and K.F. Herzfeld, *J. Chem. Phys.* **20** 1591 (1952).
14. J.T. Yardley *Introduction to Molecular Energy Transfer* (Academic, New York, 1980).
15. C.D. Holmberg, G.S. Williams, and G.P. Perram *J. Chem. Phys.* **102** 6481 (1995).
16. J. Keck and G. Carrier *J. Chem. Phys.* **43** 2284 (1965).
17. D. Rapp and T.E. Sharp *J. Chem. Phys.* **38** 2641 (1963).
18. G.P. Perram and S.J. Davis *J. Chem. Phys.* **98** 373 (1993).
19. P.J. Wolf and S.J. Davis *J. Chem. Phys.* **87** 3492 (1987).
20. J.I. Steinfeld *J. Chem. Phys.* **46** 4550 (1967).
21. G.P. Perram, D.W. Melton, T.L. Thompson, and W.B. Roh *J. Chem. Phys.* **97** 3258
22. C.W. McCurdy and W.H. Miller, *J. Chem. Phys.*, **67** 463 (1977).
23. T.A. Brunner and D. Pritchard, "Fitting Laws for Rotationally Inelastic Collisions" in *Advances in Chemical Physics, Volume 50: Dynamics of the Excited State*, edited by K.P. Lawley (John Wiley and Sons, 1982)
24. J.I. Steinfeld, P. Ruttenberg, G. Millot, G. Fanjoux, and B. Lavorel, *J. Phys. Chem.* **95**, 9638 (1991).